# Laser-induced, Surface Plasmon-enhanced Two-photon Excitation for Efficient Chemical Functionalization of Nanostructured Gold Surfaces

Kitjanit Neranon,[a] Mattias Åslund,[b] Max Yan,[c] Hao Xu,[d] Ying Fu,[e] Ingemar Petermann,[f] Per Björk,[f] and Olof Ramström*[a,g,h]

[a]Department of Chemistry, KTH - Royal Institute of Technology, Teknikringen 30, S-10044 Stockholm, Sweden; [b]BiaTect AB, Sigurdvägen 30, 182 54 Djursholm, Sweden; [c]Department of Applied Physics, KTH - Royal Institute of Technology, Hannes Alfvéns Väg 12, 11419 Stockholm, Sweden; [d]Department of Protein Science, KTH - Royal Institute of Technology, Stockholm, Sweden; [e]School of Information Technology, Halmstad University, SE-301 18 Halmstad, Sweden; [f]RISE Research Institutes of Sweden AB, Division Digital Systems, Box 1070, 164 25 Kista, Sweden; [g]Department of Chemistry, University of Massachusetts Lowell, One University Ave., Lowell, MA 01854, USA; Email: olof_ramstrom@uml.edu; [h]Department of Chemistry and Biomedical Sciences, Linnaeus University, SE-39182 Kalmar, Sweden

ABSTRACT: Functionalized gold nanostructures with efficient, broadband absorption properties are of interest for a variety of biomedical applications. In this study, we report a plasmon-enhanced functionalization methodology that results in selective surface conjugation of a fluorescent probe *via* two-photon excitation under visible-wavelength laser irradiation. The fluorescent probe was designed to incorporate a thiolated 4-piperidinyl-1,8-naphthalimide (SNaph) entity, carrying a photolabile 6-nitroveratryl (NV) protecting group, straightforwardly synthesized in a few steps in good yield. Efficient plasmon-enhanced photodeprotection of the NV-group, followed by thiol-gold bond formation on gold nanoisland substrates was recorded upon exposure to 650 nm laser light, supported by confocal laser scanning microscopy (CLSM). Photolysis of the labile NV-group, thereby efficiently exposing the free mercapto group of the thiolated 1,8-naphthalimide, was recorded upon UV-irradiation at 350 nm, whereas no cleavage occurred at 650 nm. No conjugation occurred on featureless, gold-plated flat substrates under the same conditions. Surface plasmon-enhanced two-photon excitation at plasmonic hotspots in the absorber layer thus resulted in selective and efficient conjugation of the fluorescent probe to the structured surfaces. The resulting laser-assisted approach introduces the advantage of accomplishing selective molecular functionalization at plasmonic hotspots, owing to the combined, simultaneous effects of long-wavelength deprotection and spontaneous conjugation.
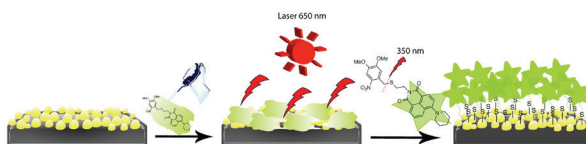
INTRODUCTION

Developments in the fields of nanoscience and nanotechnology have resulted in the emergence of a wide range of different nanostructures with unique chemical and physical properties.[1–12] Of particular interest in this context is the interaction between nanomaterials and light. Light offers a large number of advantages when applied to nanomaterials: it is straightforward to apply and can be remotely controlled both spatially and temporally; it is relatively harmless to living organisms at longer wavelengths; and it is easily implemented on various platforms, providing an efficient means to exert external stimuli.[13–21]

Combined with the fact that certain nanostructures enable control of the absorption and diffraction resonances caused by surface plasmons upon incident light excitation, a wide range of applications can be perceived. Recent advances in the fabrication of plasmonic nanomaterials have also overcome major technical challenges and resulted in the enhanced understanding and use of surface plasmons in different applications.[22–27] Engineered nanostructures thus have the ability to control surface plasmon generation, manipulation and transfer, resulting in light manipulation at the nanoscale.[28–32] For example, distinctive extinction of the spectral bands within the visible and near infrared regions can result in highly effective absorption and emission.[16,18,33] In particular, surface plasmons in the near infrared wavelength range play important roles in biological applications due to higher penetration of the skin, various tissues, and blood, accessible by light with a peak transmission at about 800 nm.[34] As a result of this development, the area of plasmonic nanostructures and nanodevices have witnessed rapid expansion and afforded a range of applications in diagnosis, imaging, therapy, communication, quantum optics, photovoltaics, catalysis, lithography, and, in particular, for chemical- and bio-sensors.[35–44] These advances have also addressed challenges concerning the diffraction limit in conventional applications.

For (bio)sensor applications, surface plasmon-enhanced two-photon excitation and associated luminescence is particularly attractive. This can result in sensitive detection, in part owing to the high signal-to-noise ratio obtained from the effective repression of the background noise. The features also enable enhanced 3D-imaging ability, and furthermore leads to minimal photodamage of organic chromophores.[46–50] In organic molecules, two-photon excitation generally ranges from the red to near-infrared region with emission wavelengths in the blue to green visible range.[51,52] Combined with the notion that two-photon excitation at near-infrared wavelengths are generally compatible with aqueous systems, and result in minimal absorption of biological chromophores, materials that enable two-photon excitation show high potential for biomedical applications. In contrast, photobleaching effects are often resulting from excitation with light at shorter wavelengths.[50,52]

Nanostructures based on noble metals possess many characteristics that make them suitable for these applications,[53–55] and have attracted considerable interest as plasmonic nanomaterials. These structures often show broadband optical absorption, which ranges from visible to near-infrared wavelengths, in combination with high chemical and physical stability.[34] The structures can be fabricated to present different sizes and shapes, and can furthermore be functionalized with a broad variety of organic molecules. Due to its high versatility and tunability, gold has proven especially suitable for the fabrication of functionalized plasmonic nanostructures, leading to an extensive exploitation in a wide range of applications,[33,34,52–56] in particular for optical sensing and imaging systems. Controllable optical properties can also be achieved with composite nanostructures thereby enabling extraordinary properties in comparison to single nanoparticles.[33] The possibility of achieving plasmonic hotspots between neighboring nanostructures is especially attractive, thereby enabling two-photon excitation at specific loci. Recently, we developed a composite, plasmonic nanostructure presenting a gold nanoisland top layer, showing efficient absorptivity throughout the visible wavelength range as well as a major portion of the near-infrared region.[57] It could be shown that the absorption efficiency depended on dipole-based resonances, resulting in the ability to amplify optical phenomena at the top surface.

Taking the benefits of light, the chemistry of photolabile entities, and the attractive features of surface plasmons for light manipulation at the nanoscale, highly efficient and selective conjugation can be achieved. This has been demonstrated in the present study, where surface plasmon-enhanced two-photon excitation at gold nanoisland films has been used to

selectively conjugate fluorescent molecular probes at plasmonic hotspots. This resulted in laser-induced, long-wavelength cleavage of photolabile protecting groups, thus exposing reactive thiol groups that enabled spontaneous bond formation on the gold surfaces. With this strategy, fluorophore-functionalized surfaces could be produced, showing the potential of generating ultrasensitive devices for bionanosensing and imaging.

RESULTS AND DISCUSSION

### Design and synthesis of fluorescent probe

The probe structure was designed to be composed of three parts: a fluorescent entity for detection, a thioalkyl chain for attachment to the gold surface, and a photolabile thiol protecting group. The 4-amino-1,8-naphthalimide motif was chosen as the fluorophore owing to its attractive chemical and photophysical properties.[58,59] This structure gives rise to internal charge transfer (ICT), with an absorption band centered around 380-450 nm, and an emission band at ca. 480-550 nm, depending on the solvent. It can furthermore be relatively easily modified through the imide- and 4-amino-groups and adapted to different applications. In the present case, a 4-piperidinyl 1,8-naphthalimide derivative was adopted for the probe entity, showing an absorption maximum at ca. 410 nm with a log ε value of 10^4 in nonpolar media.[60,61] The naphthalimide fluorophore unit was linked via an ethylene linker to the sulfur atom, which was suitably protected by the photolabile entity. A variety of light-sensitive protecting groups have for these reasons been developed,[62,63] of which the 6-nitroveratryl (NV) structure was chosen for the present setup (**Figure 1**). This structure is compatible with sulfur chemistry and displays an absorption maximum around 350 nm,[64] at which wavelength a molar extinction of 5×10^3 $M^{-1}cm^{-1}$, and a quantum yield of ~0.07 has been recorded.[65] Irradiation at around 700 nm would thus be appropriate for the deprotection process to occur only at the plasmonic hotspots. The synthetic protocol of the targeted 6-nitroveratryl-protected fluorescent naphthalimide probe (**NV-SNaph**) is shown in **Figure 1**, following a straightforward three-step sequence that resulted in a relatively high overall yield. 6-Nitroveratryl bromide **1** was first efficiently converted to compound **2** in excellent yield *via* nucleophilic substitution by cysteamine in the presence of LiOH in H_2O/EtOH.[66] Subsequently, compound **2** was condensed with 4-bromo-1,8-naphthalic anhydride **3** to afford compound **4**. Finally, nucleophilic aromatic substitution of the bromine atom at the 6-position of compound **4** in neat piperidine under refluxing conditions afforded the desired probe molecule **NV-SNaph** in moderate yield.[67]
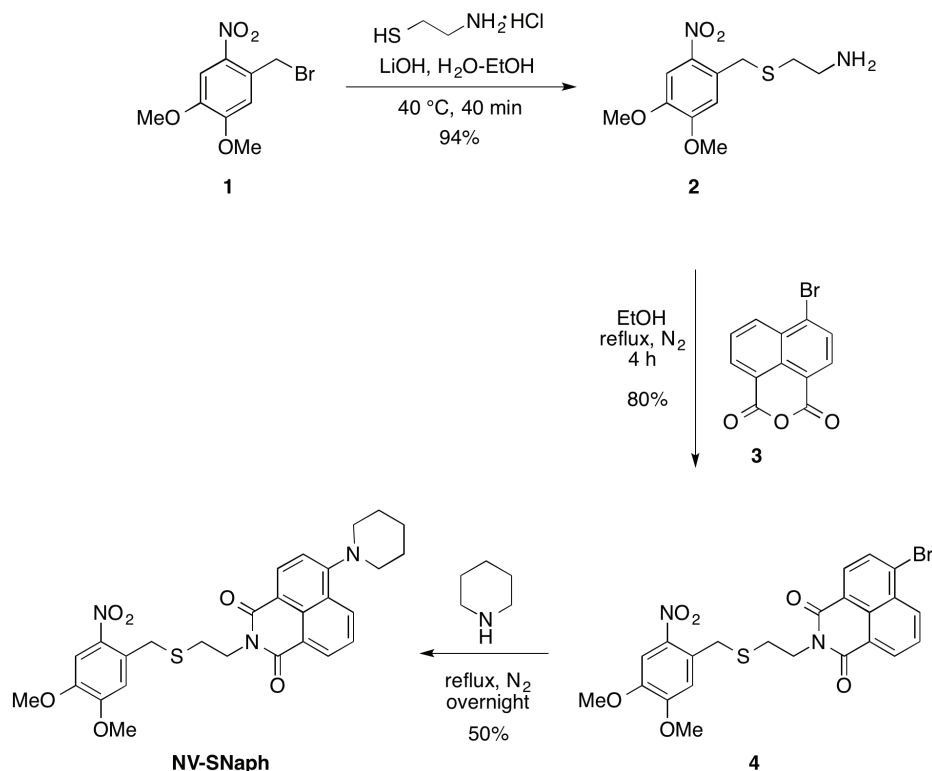
Figure 1: Synthesis of 6-nitroveratryl-protected 4-piperidinyl-1,8-naphthalimide fluorescent probe (**NV-SNaph**).

Optical properties of NV-SNaph

The spectroscopic properties, with respect to UV-Vis absorption and fluorescence, of the **NV-SNaph** probe were next evaluated, primarily assessed in chloroform solution with concentrations of ca. 10^{-5} M and 10^{-7} M, respectively. The *S*-protected cysteamine compound **2** was used as control, being devoid of the fluorescent naphthalimide group. As shown in **Figure 2** (red line), compound **2** exhibited a maximum absorption band at around 350 nm, thus showing characteristic optical properties of the 6-nitroveratryl group.[63,68] Likewise, the UV-Vis absorption spectrum of the **NV-SNaph** probe (**Figure 2**, black line), showed a distinct maximum absorption of the naphthalimide moiety at 411 nm, in accordance with data reported for similar structures.[60,61] The fluorescence emission spectrum of the **NV-SNaph** probe (λ_{ex} = 411 nm) is furthermore shown in **Figure 2** (inset), with a maximum λ_{em} at 513 nm together with very high emission intensity at the low concentration used. These results indicated the potential of the **NV-SNaph** structure to function as a fluorescent probe in this study. Upon UV-irradiation of the **NV-SNaph** probe at 350 nm, using a photochemical reactor at an intensity of 2 mW/cm^2, an increase in absorbance was observed at around 325-350 nm along with a decrease at 411 nm (**Figure 2**, blue line). This indicates photolysis of the 6-nitroveratryl group accompanied by release of the unprotected **SNaph** moiety.
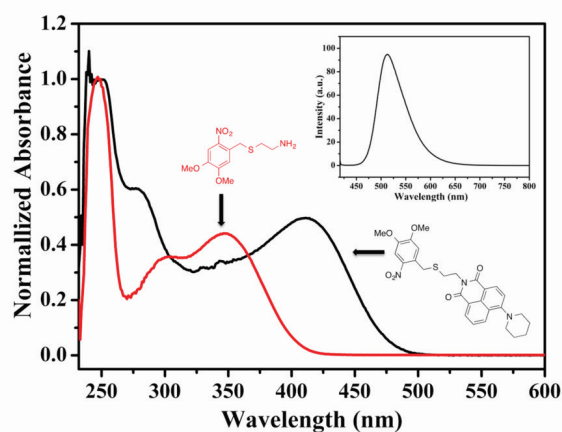
Figure 2: UV-Vis spectra of NV-SNaph (black line) compared with NV-protected thiol linkage 2 (red line). Inset: fluorescence spectrum of NV-SNaph (λ_{ex} = 411 nm).

## Photolysis of the NV-SNaph probe studied by ^{1}H-NMR- and UV-Vis-spectroscopy

As mentioned, the 6-nitroveratryl group, comprising two methoxy groups on the benzene ring, displays a maximum absorption around 350 nm and can therefore be removed with relatively long-wavelength UV light compared to other protecting groups.[62,64] The kinetics of the 6-nitroveratryl cleavage from the **NV-SNaph** probe under the influence of UV-light with a specific wavelength of 350 nm and an intensity of 1.8-2.0 mW/cm^2 was subsequently investigated. The ^{1}H-NMR spectra obtained from the resulting photolysis during 60 min at room temperature in deuterated chloroform solution are shown in **Figure** 3. As can be seen, the signal around $\delta \approx 4.19$ ppm, arising from the benzylic protons of the **NV-SNaph** probe decreased gradually, confirming successful photolysis.
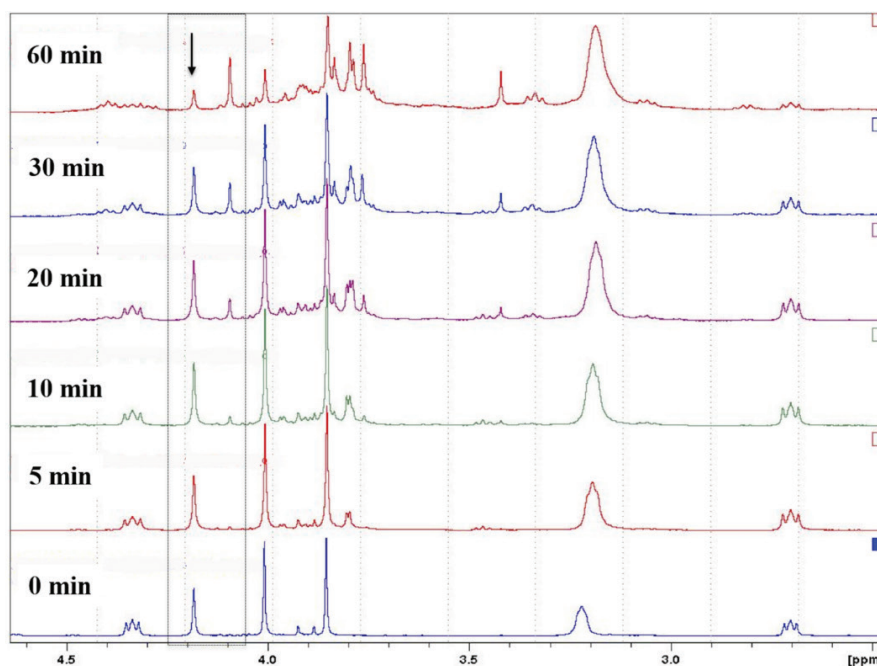
Figure 3: ^{1}H-NMR spectra of NV-SNaph in CDCl$_3$ before and after irradiation in UV photoreactor (350 nm, I = 1.8-2.0 mW/cm^2) for 0-60 min.

In addition, the kinetics of the photodeprotection of the **NV-SNaph** probe was evaluated

using UV-Vis spectroscopy to further confirm the structural change upon photolysis. In analogy to the ^{1}H NMR-study, the process was followed in chloroform solution (10^{-5} M) under exposure at 350 nm in a photochemical reactor for 1 hour (**Figure** 4). As shown in the above, the probe displayed an absorption band centered at 411 nm, characteristic of the naphthalimide moiety, as well as a band at around 300-360 nm arising from the 6-nitroveratryl moiety. Upon UV-irradiation, a slow decrease in absorption was observed at 411 nm, while the absorption at 300-360 nm gradually increased, along with a noticed color change of the solution from bright lime green to pale greenish yellow (**Figure** 4, inset). These results indicate that UV-light triggered the cleavage of the benzylic carbon-sulfur bond and provided the free *N*-thioethyl-4-piperidinyl-1,8-naphthalimide probe molecule. Thus, both ^{1}H-NMR- and UV-Vis-spectroscopy supported cleavage of the photolabile protecting 6-nitroveratryl group of the **NV-SNaph** probe under exposure to UV-light (350 nm), generating the free thiol entity linked to the fluorescent naphthalimide label.
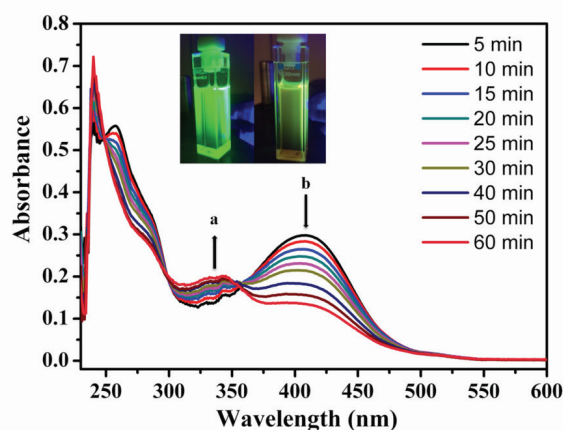

Figure 4: *UV-Vis spectra of photolysis of **NV-SNaph** (10^{-5} M) in CHCl$_3$ under irradiation in photoreactor (350 nm, I = 2.8-3.2 mW/cm^2) for 0-60 min. Inset: fluorescence color change of **NV-SNaph** (1.7 mg/mL) before (left) and after (right) 350 nm UV-irradiation for 30 min.*

## Gold surface functionalization through UV-triggered cleavage of the NV-SNaph probe

Having evaluated the photolysis of the 6-nitroveratryl moiety of the **NV-SNaph** probe in solution, the light-induced functionalization of flat, featureless gold surfaces was investigated (*cf.* supporting information). It was expected that deprotection and conjugation would occur at 350 nm, whereas the 6-nitroveratryl group would be stable at the double wavelength. To visualize the chemical conjugation of the fluorescent probe onto the substrates resulting from photolysis of the carbon-sulfur bond of the **NV-SNaph** probe, confocal laser scanning microscopy (CLSM) was applied and the fluorescence images evaluated. Three different conditions were thus assessed: no irradiation, irradiation at 350 nm, and irradiation at 650 nm, respectively. The confocal images of the surfaces not having been exposed to any irradiation showed strong residual fluorescence at both the quartz- and gold-areas of the crystal before washing (**Figure** 5a), however easily removed upon washing by dichloromethane (soaking overnight) to remove the physisorbed and/or excess amount of probes (**Figure** 5b). The same results were obtained from crystals irradiated by laser light at 650 nm, with no fluorescence detected after washing/soaking in dichloromethane (**Figure** 5c). However, as expected, strong, residual, green fluorescence of the *N*-thioethyl-4-piperidinyl-1,8-naphthalimide probe was observed on the gold surfaces following irradiation at 350 nm and washing/soaking overnight (**Figure** 5d-e), whereas largely no fluorescence was observed on the quartz areas of

the crystals. These results imply that the protected fluorescent probe could be deprotected by irradiation at 350 nm, and subsequently chemisorbed on the gold surfaces *via* thiol-Au bond formation. Any physisorbed fluorophores could be easily removed by washing, after which only trace amounts were observed.
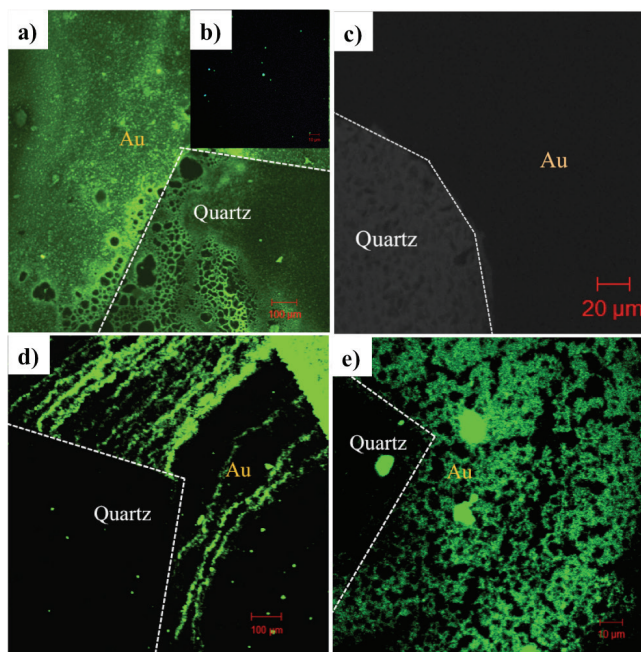
Figure 5: *CLSM images of gold-plated quartz crystal substrates treated with the **NV-SNaph** probe. a) without irradiation before washing (10X); b) idem after washing (63X); c) irradiation by 650 nm laser for 30 min and washing (40X); d) irradiation at 350 nm for 30 min and washing (10X); e) idem (63X).*

The hypothesis of using gold nanoisland surfaces to achieve two-photon excitation and chemical conjugation at plasmonic hotspots was next tested. The gold-nanoisland substrates were thus exposed to concentrated solutions of the **NV-SNaph** probe and further evaluated using the CLSM technique. The results were in this case very clear, and irradiation at either 650 or 350 nm resulted in strong, residual fluorescence, which could not be removed by washing (**Figure 6b-c**). This indicates efficient cleavage of the 6-nitroveratryl group followed by covalent ligation of the fluorescent naphthalimide probe onto the gold-nanoisland surfaces. In addition, a higher and more uniform coverage of the naphthalimide fluorophore was obtained upon laser irradiation at 650 nm (**Figure 6c-d**), compared to the results from irradiation at 350 nm (**Figure 6b**). In contrast, only trace residual fluorescence could be observed at non-irradiated substrates used as a control after washing/soaking in dichloromethane overnight (**Figure 6a**). This supports photolysis of the **NV-SNaph** probe, assisted by plasmon-enhanced two-photon excitation for ultimate gold-surface functionalization. Comparison of the results obtained from both types of gold substrates indicates that featured gold-nanoisland surfaces are required to result in conjugation at higher wavelengths. Although the 6-nitroveratryl protecting group cannot be directly cleaved using irradiation by laser light at 650 nm, where the wavelength is outside the excitation band, the gold-nanoisland surfaces can produce a plasmonic effect resulting in energy at half the wavelength ($\lambda/2$) of the source (around 325 nm). Thereby, the photolabile protecting group can be removed, and the thioethyl-derivatized naphthalimide fluorophore become attached to the gold surfaces.
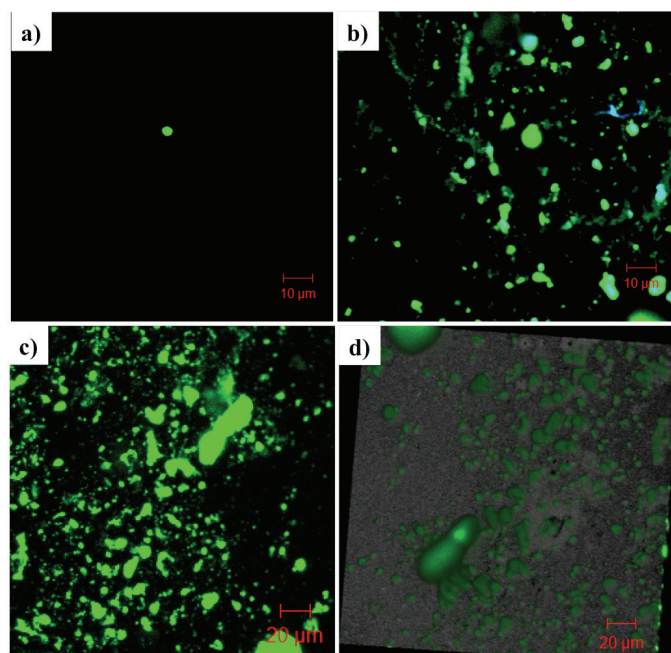
Figure 6: *CLSM images of gold nanoisland substrates treated with the **NV-SNaph** probe. a) no irradiation (63X); b) irradiation at 350 nm for 30 min (63X); c) irradiation at 650 nm for 30 min (40X); d) irradiation at 650 nm for 30 min, 3D-image (40X).*

CONCLUSIONS

We have developed a new chemisorption approach by which nanostructured gold surfaces endowed with broadband plasmon absorption can be efficiently functionalized with photocaged molecules. Laser-induced surface plasmon-enhanced cleavage of a photolabile protecting group efficiently generated free thiols, which underwent spontaneous covalent attachment of the uncaged entity through sulfur-gold bond formation. This could be demonstrated by conjugation of an *N*-thioethylated 1,8-naphthalimide fluorophore, originally protected by a 6-nitroveratryl group. Irradiation of the caged fluorophore at the surfaces, at a longer wavelength otherwise inefficient for deprotection, resulted in fluorescently-labeled gold-nanoisland surfaces. This represents the first demonstration of using plasmon-enhanced two-photon excitation for covalent conjugation at plasmonic hotspots. These results not only point to the possibility of achieving ultrasensitive sensor devices, but also promote further development of plasmonic nanostructure functionalization with various biomolecules, leading to a variety of applications in the biomedical field.

EXPERIMENTAL

General

Piperidine was from Alfa Aesar, anhydrous lithium hydroxide was from Lancaster, and cysteamine hydrochloride, 4,5-dimethoxy-2-nitrobenzyl bromide, and 4-bromo-1,8-naphthalic anhydride were from Sigma Aldrich. HPLC-grade ethanol, methanol, dichloromethane, ethyl acetate, and hexane were used throughout. Water used was from a deionization water purification system. Gold-nanoisland-featured, three-layer plasmonic nanostructures were prepared as previously reported,[57] composed of a gold nanoparticle layer on top of a thin layer of Al_2O_3, and a reflecting layer of gold, mounted on a silicon substrate. Flat, featureless,

gold-plated quartz crystals were from Attana AB. NMR data were recorded on a Bruker DMX 500 spectrometer at 500 MHz (^{1}H) and 126 MHz (^{13}C). Chemical shifts (δ) are reported in parts per million (ppm) values with residual CHCl$_3$ (^{1}H: δ = 7.26) or CDCl$_3$ (^{13}C = 77.16) as internal references. J-values are given in hertz (Hz). Melting points (uncorrected) were recorded using a Stuart SMP10 melting point apparatus. Thin layer chromatography (TLC) was performed on precoated Cromatofolios AL Silica gel 60 F254 plates (Merck). ESI-MS spectra were recorded in positive mode on a Finnigan LCQ Advantage Max: LC-MS/MS spectrometer (Thermo Fisher Science) with sample analysis through standard ESI+ acquisition parameters. UV-Vis absorption spectra were collected on a Varian Cary 300 Bio UV/Vis spectrophotometer. Emission spectra were recorded on a Varian Cary Eclipse fluorescence spectrophotometer. Irradiation was performed with a photochemical reactor from Rayonet Srinivasan-Griffin emitting at 350 nm or a 650 nm laser pointer with an intensity of 2 mW·cm^{-2}. Confocal imaging was carried out using a Zeiss Laser Scanning Microscope 510 Zuidhorst 178 equipped with Zen software and 10x and 63x air objectives. FT-IR spectra were obtained using a PerkinElmer IR-spectrometer SPECTRUM 2000 in the ATR mode.

Synthesis

2-((4,5-Dimethoxy-2-nitrobenzyl)thio)ethan-1-amine (Compound 2).[66] LiOH (17 mg, 0.72 mmol) was dissolved in water (1 mL) and ethanol (3 mL) was added. The resulting solution was added to cysteamine hydrochloride (41 mg, 0.36 mmol) followed by dropwise addition of 6-nitroveratryl bromide (**1**) (100 mg, 0.36 mmol) under stirring. The reaction mixture was stirred for 40 min at 40 °C, after which ethanol was removed *in vacuo*. Water (5 mL) was subsequently added and the mixture was extracted with dichloromethane (3 × 10 mL), dried over anhydrous Na$_2$SO$_4$, concentrated *in vacuo*, and purified by flash column chromatography over silica gel (60Å, 0.040-0.063 mm (SDS) using a mobile phase consisting of a mixture of dichloromethane-methanol (gradient from 2% v/v methanol/dichloromethane to 10% v/v methanol/dichloromethane) to afford pure compound **2** (93 mg, 94%). ^{1}H NMR (500 MHz, CDCl$_3$): δ_{ppm} 7.59 (s, 1H, Ar-*H*), 6.93 (s, 1H, Ar-*H*), 4.10 (s, 2H, Ar-C*H$_2$*), 3.96 (s, 3H, O-C*H$_3$*), 3.92 (s, 3H, O-C*H$_3$*), 2.91 (brs, 2H, N-C*H$_2$*), 2.64 (t, 2H, J = 6.5 Hz, S-C*H$_2$*). ^{13}C NMR (126 MHz, CDCl$_3$): δ_{ppm} 153.0, 147.9, 140.9, 129.0, 113.2, 108.5, 56.5, 56.4, 41.1, 36.4, 33.6. mp: 91-93 °C. ESI-MS (positive mode): Calcd for C$_{11}$H$_{16}$N$_2$O$_4$S: [M+H]$^+$ m/z = 273.0909. Found: [M+H]$^+$ m/z = 273.0667. FT-IR (ATR, neat): See Supporting Information.

6-Bromo-2-(2-((4,5-dimethoxy-2-nitrobenzyl)thio)ethyl)-1*H*-benzo[*de*]isoquinoline-1,3(2*H*)-dione (Compound 4). A mixture of 6-bromo-1*H*,3*H*-benzo[*de*]isochromene-1,3-dione (**3**) (95 mg, 0.34 mmol) and compound **2** (93 mg, 0.34 mmol) in ethanol (5 mL) was heated under reflux for 4 h, and then cooled down to room temperature followed by storage in a freezer overnight. After isolation by filtration and drying, compound **4** was obtained as a white powder (145 mg, 80%). ^{1}H NMR (500 MHz, CDCl$_3$): δ_{ppm} 8.62 (d, 1H, J = 7.5 Hz, Naph-*H*), 8.60 (d, 1H, J = 8.0 Hz, Naph-*H*), 8.38 (d, 1H, J = 8.0 Hz, Naph-*H*), 8.06 (d, 1H, J = 7.5 Hz, Naph-*H*), 7.86 (t, 1H, J = 8.0 Hz, Naph-*H*), 7.64 (s, 1H, Ar-*H*), 7.12 (s, 1H, Ar-*H*), 4.39 (t, 2H, J = 7.6 Hz, N-C*H$_2$*), 4.24 (s, 2H, Ar-C*H$_2$*), 4.07 (s, 3H, O-C*H$_3$*), 3.91 (s, 3H, O-C*H$_3$*), 2.80 (t, 2H, J = 7.6 Hz, S-C*H$_2$*). ^{13}C NMR (126 MHz, CDCl$_3$): δ_{ppm} 163.5, 163.5, 152.9, 147.8, 140.3, 133.6, 132.1, 131.3, 131.2, 130.7, 130.6, 129.6, 129.1, 128.2, 122.9, 122.0, 113.9, 108.9, 56.6, 56.4, 39.8, 34.0, 28.9. mp: 206-208 °C. ESI-MS (positive mode): Calcd for C$_{23}$H$_{19}$BrN$_2$O$_6$S: [M+Na]$^+$ m/z = 553.0045. Found: [M+Na]$^+$ m/z = 553.1333. FT-IR (ATR, neat): See Supporting Information.

2-(2-((4,5-Dimethoxy-2-nitrobenzyl)thio)ethyl)-6-(piperidin-1-yl)-1*H*-benzo[*de*]isoquinoline-1,3(2*H*)-dione (NV-SNaph).[67] Compound **4** (50 mg, 0.094 mmol) was heated to reflux in piperidine (2.5 mL) overnight under a nitrogen stream. The solvent was removed *in vacuo* and the resulting residue purified by flash column chromatography over silica gel (60Å, 0.040-0.063 mm (SDS) using a mobile phase consisting of a mixture of hexane-ethyl acetate (gradient from 30% v/v ethyl acetate/hexane to 100% v/v acetate/hexane) to give **NV-SNaph** as a yellow solid (26 mg, 50%). ^{1}H NMR (500 MHz, CDCl$_3$): δ_{ppm} 8.54 (d, 1H, J = 7.5 Hz, Naph-*H*), 8.47-8.43 (m, 2H, Naph-*H*), 7.70 (d, 1H, J = 7.5 Hz, Naph-*H*), 7.68 (s, 1H, Ar-*H*), 7.20 (d, 1H, J = 8.0 Hz, Naph-*H*), 7.18 (s, 1H, Ar-*H*), 4.40 (t, 2H, J = 7.5 Hz, N-C*H$_2$*), 4.25 (s, 2H, Ar-C*H$_2$*), 4.08 (s, 3H, O-C*H$_3$*), 3.92 (s, 3H, O-C*H$_3$*), 3.26 (brs, 4H, 2xN$_{pip}$-C*H$_2$*), 2.76 (t, 2H, J = 7.5 Hz, S-C*H$_2$*), 1.92 (brs, 4H, 2xN$_{pip}$CH$_2$-C*H$_2$*), 1.74 (brs, 2H, N$_{pip}$CH$_2$CH$_2$-C*H$_2$*). ^{13}C NMR (126 MHz, CDCl$_3$): δ_{ppm} 164.4, 163.9, 152.9, 147.8, 140.2, 132.6, 131.2, 130.9, 130.0, 129.9, 126.2, 125.6, 122.9, 115.0, 114.1, 109.0, 56.6, 56.4, 54.7, 39.5, 33.8, 29.7, 28.7, 26.0, 24.2. mp: 160-162 °C. ESI-MS (positive mode): Calcd for C$_{28}$H$_{29}$N$_3$O$_6$S: [M+Na]$^+$ m/z = 558.1669. Found: [M+Na]$^+$ m/z = 558.4000. FT-IR (ATR, neat): See Supporting Information.

NV-SNaph photolysis

NMR: A solution of **NV-SNaph** in CDCl$_3$ (10 mg/mL) in an NMR tube was placed inside a photochemical reactor and irradiated at 350 nm with an intensity of 1.8-2.0 mWcm^{-2}. At specific time intervals, ^{1}H-NMR spectra were recorded at room temperature. UV-Vis: A solution of **NV-SNaph** in chloroform (10^{-5} M) in a quartz cuvette was irradiated at 350 nm in a photochemical reactor at an intensity of 2.8-3.2 mWcm^{-2} for 1 hour. Absorption spectra were collected at specific irradiation times at a wavelength range from 225 to 600 nm.

Photoinduced surface functionalization

A solution of **NV-SNaph** in dichloromethane (10 mg/mL) was dropped onto the gold-plated quartz crystal surfaces (50 µL) and gold-nanoisland substrates (100 µL), after which the surfaces were dried under vacuum overnight. The non-irradiated control samples were subsequently washed with dichloromethane several times and then soaked in dichloromethane overnight to remove all physisorbed **NVB-SNaph** on the surfaces. The remaining samples were first irradiated at 350 or 650 nm (I = 2 mWcm^{-2}) for 30 min, and subsequently left under an N$_2$ flow for several hours, followed by washing with dichloromethane in the same way as with the control samples. All samples were finally dried under vacuum overnight before the CLSM experiments.

AUTHOR INFORMATION

Corresponding Author

Olof Ramström; E-mail: olof_ramstrom@uml.edu

REFERENCES

[1] M.-H. Seo, J.-Y. Yoo, M.-S. Jo, J.-B. Yoon, *Adv. Mater.* **2020**, *32*, 1907082.

[2] Y.-P. Xie, Y.-L. Shen, G.-X. Duan, J. Han, L.-P. Zhang, X. Lu, *Mater. Chem. Front.* **2020**, *4*, 2205–2222.

[3] G. Xie, M. R. Martinez, M. Olszewski, S. S. Sheiko, K. Matyjaszewski, *Biomacromolecules* **2019**, *20*, 27–54.

[4] N. Panwar, A. M. Soehartono, K. K. Chan, S. Zeng, G. Xu, J. Qu, P. Coquet, K.-T. Yong, X. Chen, *Chem. Rev.* **2019**, *119*, 9559–9656.

[5] J. Leng, Z. Wang, J. Wang, H.-H. Wu, G. Yan, X. Li, H. Guo, Y. Liu, Q. Zhang, Z. Guo, *Chem. Soc. Rev.* **2019**, *48*, 3015–3072.

[6] Z. Xi, H. Ye, X. Xia, *Chem. Mater.* **2018**, *30*, 8391–8414.

[7] M. Qiu, W. X. Ren, T. Jeong, M. Won, G. Y. Park, D. K. Sang, L.-P. Liu, H. Zhang, J. S. Kim, *Chem. Soc. Rev.* **2018**, *47*, 5588–5601.

[8] L. Liu, Y. Zhou, S. Liu, M. Xu, *ChemElectroChem* **2018**, *5*, 6–19.

[9] H. Lin, Y. Chen, J. Shi, *Chem. Soc. Rev.* **2018**, *47*, 1938–1958.

[10] C. Cheng, S. Li, A. Thomas, N. A. Kotov, R. Haag, *Chem. Rev.* **2017**, *117*, 1826–1914.

[11] S. Mao, J. Chang, H. Pu, G. Lu, Q. He, H. Zhang, J. Chen, *Chem. Soc. Rev.* **2017**, *46*, 6872–6904.

[12] G. Wen, Z. Guo, W. Liu, *Nanoscale* **2017**, *9*, 3338–3366.

[13] R. Gordon, *Nanotechnology* **2019**, *30*, 212001.

[14] L. Wang, Q. Li, *Chem. Soc. Rev.* **2018**, *47*, 1044–1097.

[15] X. Li, S. Lee, J. Yoon, *Chem. Soc. Rev.* **2018**, *47*, 1174–1188.

[16] D. G. Baranov, M. Wersäll, J. Cuadra, T. J. Antosiewicz, T. Shegai, *ACS Photonics* **2018**, *5*, 24–42.

[17] P. Vasa, C. Lienau, *ACS Photonics* **2018**, *5*, 2–23.

[18] S. Kundu, A. Patra, *Chem. Rev.* **2017**, *117*, 712–757.

[19] S. Yu, X. Wu, Y. Wang, X. Guo, L. Tong, *Adv. Mater.* **2017**, *29*, 1606128.

[20] Y. Zang, J. Lei, H. Ju, *Biosens. Bioelectron.* **2017**, *96*, 8–16.

[21] A. Kristensen, J. K. W. Yang, S. I. Bozhevolnyi, S. Link, P. Nordlander, N. J. Halas, N. A. Mortensen, *Nat. Rev. Mater.* **2016**, *2*, 16088.

[22] X. Wang, S.-C. Huang, S. Hu, S. Yan, B. Ren, *Nat. Rev. Phys.* **2020**, *2*, 253–271.

[23] P. Zhang, D. Wang T., J. Gong, *Adv. Mater.* **2015**, *27*, 5328–5342.

[24] P. N. Abadian, C. P. Kelley, E. D. Goluch, *Anal. Chem.* **2014**, *86*, 2799–2812.

[25] M. R. Gonçalves, *J. Phys. D: Appl. Phys.* **2014**, *47*, 213001.

[26] E. C. A. Stigter, G. J. de Jong, W. P. van Bennekom, *Trends Anal. Chem.* **2013**, *45*, 107–120.

[27] C. M. Galloway, M. P. Kreuzer, S. S. Aćimović, G. Volpe, M. Correia, S. B. Petersen, M. T. Neves-Petersen, R. Quidant, *Nano Lett.* **2013**, *13*, 4299–304.

[28] J. Cunha, T.-L. Guo, G. Della Valle, A. N. Koya, R. Proietti Zaccaria, A. Alabastri, *Adv. Opt. Mater.* **2020**, *8*, 2001225.

[29] H. Song, H. Ahn, T. Kim, Y. Lee, J.-R. Choi, K. Kim, *Appl. Spectrosc. Rev.* **2019**, *54*, 482–508.

[30] C. Bradac, *Adv. Opt. Mater.* **2018**, *6*, 1800005.

[31] H. Wei, H. Xu, *Mater Today* **2014**, *17*, 372–380.

[32] O. M. Maragò, P. H. Jones, P. G. Gucciardi, G. Volpe, A. C. Ferrari, *Nat. Nanotechnology* **2013**, *8*, 807–819.

[33] M. Achermann, *J. Phys. Chem. Lett.* **2010**, *1*, 2837–2843.

[34] A. Poletti, G. Fracasso, G. Conti, R. Pilot, V. Amendola, *Nanoscale* **2015**, *7*, 13702–14.

[35] L. K. Chin, T. Son, J.-S. Hong, A.-Q. Liu, J. Skog, C. M. Castro, R. Weissleder, H. Lee, H. Im, *ACS Nano* **2020**, *14*, 14528–14548.

[36] V. T. Tran, H.-Q. Nguyen, Y.-M. Kim, G. Ok, J. Lee, *Nanomaterials* **2020**, *10*, 1–19.

[37] Y. Mantri, J. V. Jokerst, *ACS Nano* **2020**, *14*, 9408–9422.

[38] V. De Matteis, L. Rizzello, M. Cascione, E. Liatsi-Douvitsa, A. Apriceno, R. Rinaldi, *Nanomaterials* **2020**, *10*, 1083.

[39] C. Li, Y. Jin, *Adv. Funct. Mater.* **2020**, 2008031.

[40] Z. Li, L. Leustean, F. Inci, M. Zheng, U. Demirci, S. Wang, *Biotechnol. Adv.* **2019**, *37*, 107440.

[41] M. Sharifi, F. Attar, A. A. Saboury, K. Akhtari, N. Hooshmand, A. Hasan, M. A. El-Sayed, M. Falahati, *J. Controlled Release* **2019**, *311-312*, 170–189.

[42] F. Hong, R. Blaikie, *Adv. Opt. Mater.* **2019**, *7*, 1801653.

[43] J. D. Spitzberg, A. Zrehen, X. F. van Kooten, A. Meller, *Adv. Mater.* **2019**, *31*, 1900422.

[44] A. Prasad, J. Choi, Z. Jia, S. Park, M. R. Gartia, *Biosens. Bioelectron.* **2019**, *130*, 185–203.

[45] X. Ma, S. J. Sim, *J. Mater. Chem. B* **2020**, *8*, 6197–6216.

[46] H. Zong, X. Mu, M. Sun, *Appl. Mater. Today* **2019**, *15*, 43–57.

[47] W. Park, D. Lu, S. Ahn, *Chem. Soc. Rev.* **2015**, *44*, 2940–2962.

[48] J. Zhou, Q. Liu, W. Feng, Y. Sun, F. Li, *Chem Rev* **2015**, *115*, 395–465.

[49] R.-Y. He, Y.-D. Su, K.-C. Cho, C.-Y. Lin, N.-S. Chang, C.-H. Chang, S.-J. Chen, *Opt. Express* **2009**, *17*, 5987.

[50] D.-S. Wang, F.-Y. Hsu, C.-W. Lin, *Opt. Express* **2009**, *17*, 11350.

[51] H. M. Kim, B. R. Cho, *Chem. Rev.* **2015**, *115*, 5014–5055.

[52] J. H. Lin, C.-Y. Tseng, C.-T. Lee, H.-C. Kan, C. C. Hsu, *Opt. Express* **2013**, *21*, 24318–25.

[53] G. V. Hartland, L. V. Besteiro, P. Johns, A. O. Govorov, *ACS Energy Lett.* **2017**, *2*, 1641–1653.

[54] A. J. Wilson, K. A. Willets, *Annu. Rev. Anal. Chem.* **2016**, *9*, 27–43.

[55] J.-C. Tinguely, I. Sow, C. Leiner, J. Grand, A. Hohenau, N. Felidj, J. Aubard, J. R. Krenn, *Bionanoscience* **2011**, *1*, 128–135.

[56] P. Tiwari, K. Vig, V. Dennis, S. Singh, *Nanomaterials* **2011**, *1*, 31–63.

[57] M. Yan, J. Dai, M. Qiu, *J. Opt.* **2014**, *16*, 025002.

[58] R. M. Duke, E. B. Veale, F. M. Pfeffer, P. E. Kruger, T. Gunnlaugsson, *Chem. Soc. Rev.* **2010**, *39*, 3936.

[59] Y. Q. Gao, R. A. Marcus, *J. Phys. Chem. A* **2002**, *106*, 1956–1960.

[60] S. Saha, A. Samanta, *J. Phys. Chem. A* **2002**, *106*, 4763–4771.

[61] A. Peters, *Dye. Pigment.* **1985**, *6*, 349–375.

[62] M. J. Hansen, W. A. Velema, M. M. Lerch, W. Szymanski, B. L. Feringa, *Chem. Soc. Rev.* **2015**, *44*, 3358–77.

[63] C. G. Bochet, *Angew. Chem. Int. Ed.* **2001**, *40*, 2071–2073.

[64] A. Patchornik, B. Amit, R. B. Woodward, *J. Am. Chem. Soc.* **1970**, *92*, 6333–6335.

[65] J. P. Casey, R. A. Blidner, W. T. Monroe, *Mol. Pharm.* **2009**, *6*, 669–685.

[66] S. Ghosh, G. P. Tochtrop, *Tetrahedron Lett.* **2009**, *50*, 1723–1726.

[67] C. J. McAdam, J. L. Morgan, B. H. Robinson, J. Simpson, P. H. Rieger, A. L. Rieger, *Organometallics* **2003**, *22*, 5126–5136.

[68] A. Blanc, C. G. Bochet, *J. Org. Chem.* **2002**, *67*, 5567–5577.